THE JOURNAL OF PHYSICAL CHEMISTRY Letters

LETTER

pubs.acs.org/JPCL

Spectrally Resolved Photoluminescence Imaging of ZnO Nanocrystals at Single-Particle Levels

Arunasish Layek,* Suman De, Ruhi Thorat, and Arindam Chowdhury*

Department of Chemistry and National Center for Photovoltaic Research and Education (NCPRE), Indian Institute of Technology Bombay, Mumbai 400076, India.

Supporting Information

ABSTRACT: The intrinsic spectral line widths of defect-related transitions in quantum-confined semiconductor nanocrystals are often difficult to estimate using ensemble measurements because the extent of inhomogeneous broadening due to particle size distributions is not known precisely. To address this problem, we performed spectrally resolved photoluminescence (PL) microscopy of individual ZnO NC by directly populating the defects states using low-energy laser excitation. The temporal evolution of PL intensities shows discrete blinking behaviors, suggesting that the NCs are detected near single-particle levels. The transition energies of individual NCs are found to fluctuate around their mean position (2.25 eV) by ~0.130 eV, which is attributed to particle size distribution and defects densities associated with each NC. The spectral line width associated with defect emission envelope of ZnO NCs is found to be inherently broad (200−400 meV), which further establishes the presence of multiple closely spaced defect energy levels within every ZnO NC.

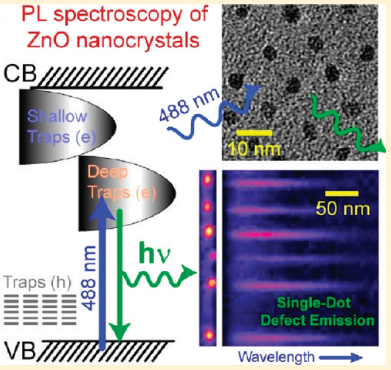

SECTION: Nanoparticles and Nanostructures

Among the naturally occurring wide band gap semiconductors, ZnO comes to the forefront owing to its direct wide band gap (~3.37 eV) with large exciton binding energy (60 meV).[1] ZnO is considered to be one of the most technologically promising semiconducting materials with a variety of applications as chemical sensors, photocatalysts, UV laser diodes, phosphors, photovoltaic devices, and sunscreen skin protection gels.[2−4] Moreover, the relative ease of synthesis, size-selection, and easy surface modification of ZnO nanocrystals (NCs) has fueled their potential as luminescent biomarkers for in vivo imaging.[5−7] For ZnO NCs synthesized using colloidal chemical routes, in addition to the weak excitonic photoemission in the UV, a broad defect-related visible luminescence having a Stokes shift of 1 to 1.6 eV is observed under ambient conditions. It has been shown that depending on the preparation techniques, capping groups, NC dimensions, crystal morphology, surface-to-volume ratio, and so on, defect states in ZnO can have very different radiative recombination dynamics resulting in energetic and intensity changes for the visible emission.[8−12] There is a general consensus that low-lying radiative trap states are created because of structural defects at the surface (such as dangling bonds and hydroxo-/peroxo- linkages, etc.) as well as native point defects (such as vacancies, Zn antisite/interstices, oxygen antisite/interstices) that trap carriers efficiently, and the broad visible emission arises from tunneling recombination of donor−acceptor pairs.[2,9,13−21] It should be pointed out that a large number of recent reports have shown that the broad visible emission is actually composed of multiple defect related transitions.[2,9,11,12,20−22] However, it is still ambiguous whether this emission band is a result of several closely spaced transitions inherent of every ZnO NC or arises because of particle-size distributions of NCs each having energetically distinct but relatively narrow line widths.

It is difficult to characterize the line widths of various defect transitions using ensemble photoluminescence (PL) measurements because the contribution of NC size distributions on the overall spectral widths cannot be obtained in a straightforward manner. Conversely, if photophysical properties of NCs can be probed at single-particle level, then it is possible to decouple such inhomogeneous broadening effects arising from particle-size distributions. Single-molecule fluorescence microscopy (SMFM) has emerged as an extremely powerful tool for imaging and probing the dynamics of individual fluorescent molecules, and luminescent semiconductor nanocrystals (Quantum-Dots).[23−26] Imaging and spectroscopy of individual NCs have revealed interesting optoelectronic behaviors such as PL intermittency (blinking) and spectral diffusion, which cannot be obtained using ensemble measurements.[26−29] However, SMFM measurements on wide band gap semiconductors like ZnO require UV excitation sources, which is challenging because of autofluorescence of microscope optics and the presence of fluorescence impurities that could be excited in the UV. This problem

Received: March 18, 2011
Accepted: May 2, 2011

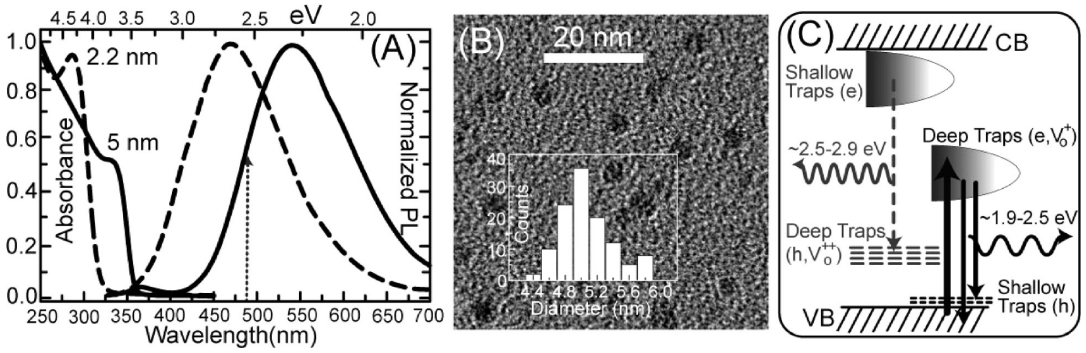

Figure 1. (A) UV−vis absorption and PL spectra of 2.2 (dashed) and 5 nm (solid) diameter ZnO NCs in methanol solution. (B) TEM image of the larger ZnO NCs and size distribution (inset) obtained from the analysis of more than 100 particles. (C) Defect-related transitions responsible for the broad visible emission in ZnO NCs (based on refs 16, 17, and 22).

can be circumvented if the defect states of ZnO are populated using laser excitation in the visible region.

Recently, a few reports have shown that the defects of ZnO NCs can be excited using visible laser irradiation to obtain PL spectra originating from carrier recombination through several surface related and native defects lying between the valence band (VB) and conduction band (CB).[6,14,30−32] This implies that carriers can be generated directly in the defect states of the NCs by photoexcitation at energies much lower than the band gap. Utilizing this methodology, attempts have been made to successfully image surface-modified ZnO NCs inside plant cells.[6] However, to the best of our knowledge, there are no reports on PL microscopy of ZnO NCs at (or near) single-particle levels. This motivated us to perform PL imaging measurements of individual ZnO NCs using a 488 nm laser excitation. This Letter demonstrates that it is possible to image ZnO NCs, monitor their blinking behaviors, and concurrently obtain their spectrally resolved emission profiles at or near single-particle levels. Our results show that the red-edge of the visible defect emission is intrinsically broad and is characteristic of each ZnO NC, and energetic shifts due to particle size distributions do not contribute significantly to the defect emission line widths observed in the ensemble.

Figure 1A shows the optical absorption spectra of the TBPA-capped colloidal ZnO nanocrystals of two distinct sizes in methanol. The sharp onset of the excitonic absorption indicates narrow size distributions for both the large and small NCs. The particle sizes estimated from the excitonic absorption profile using tight-binding model (TBM) calculations were found to be ∼2.2 and ∼5 nm having a size distribution of <20%.[33,34] Figure 1B shows a TEM image of larger quasi-spherical particles, whereas electron diffraction and X-ray diffraction patterns (Supporting Information, Figure S1) confirm the formation of wurtzite ZnO NCs. The size distribution obtained from the analyses of TEM images (Figure 1B, inset) shows that the vast majority of ZnO NCs have diameters between 4.4 and 5.8 nm. The mean size of 5.04 nm obtained from the TEM size distribution was found to be consistent with the size estimates from TBM calculations.

The steady-state PL spectra (λ_{ex} = 320 nm) of the same samples in methanol solution shows the presence of two emission bands (Figure 1A). The weak transition in the UV (∼360 nm) is due to excitonic near band-edge emission, whereas the intense red-shifted band spanning the entire visible range is ascribed to impurity-related (deep level defects) transitions.[8,16] As observed in Figure 1A and also previously reported by several groups, this broad defect emission envelope red-shifts with increasing NC size.[18,35] This suggests that the defect states are associated with the VB or CB of the NCs and follows analogous energetic shifts with the degree of excitonic confinement. It should be noted that this broad visible emission band has at least two (probably more) contributions (Figure 1C) originating from surface-defect-related states such as deep-acceptor levels for holes (V_o^{++}) and deep-donor levels for electrons (V_o^{+}). It is believed that the recombination of electrons from CB edge (tail states or shallow traps) with holes in V_o^{++} is responsible for the blue-edge of the defect emission, whereas the red-edge in the visible envelope is due to recombination of deeply trap electrons (V_o^{+}) with free VB holes or holes in shallow traps.[9,16−18,22] It should be noted that both these bands in turn are believed to consist of several transitions due to the presence of multiple close-lying defect energy levels through which carriers can recombine radiatively.[3,9,10,17,21] Interestingly, it has been shown that some of these trap states in ZnO nanostructures can be excited at energies lower than the band gap.[6,14,31,32] Moreover, it was even possible to obtain the PL emission spectra originating from these traps by directly populating some of the defect states.[14,31]

The larger (∼5 nm) ZnO sample was chosen for PL imaging measurements because their emission maximum in solution was ∼540 nm, which allows for the collection of majority of the visible emission between 500 and 700 nm. Figure 2A shows the PL image of only the capping group (5 nM TBPA) in methanol in the absence of any ZnO NC. This image shows the presence of a few luminescent spots, having intensities well above the background signal, and is attributed to fluorescent impurities in the solvent (or in TBPA). Figure 2B−C shows PL images of ZnO NCs spin-cast out of methanol at two different concentrations (∼400 pM and ∼2 nM) while keeping all other parameters (such as solvent, spin-coating conditions, excitation powers, and exposure times) unchanged. These images show the presence of highly localized luminescent spots, which were found to scale with increasing concentration of ZnO in solution. These spots are attributed to ZnO NCs. It should be noted that the emission intensities of each spot was found to be significantly less than that of single-fluorescent dye molecules such as Perylenebisimide (PBI) or Rhodamine6G (Rh6G) under similar conditions. For instance, Figure 2A−C was obtained at exposure time of 1 s, whereas single PBI or Rh6G molecules can be easily imaged at few ms exposure times under identical excitation power. It is also evident that relatively high power densities are required for

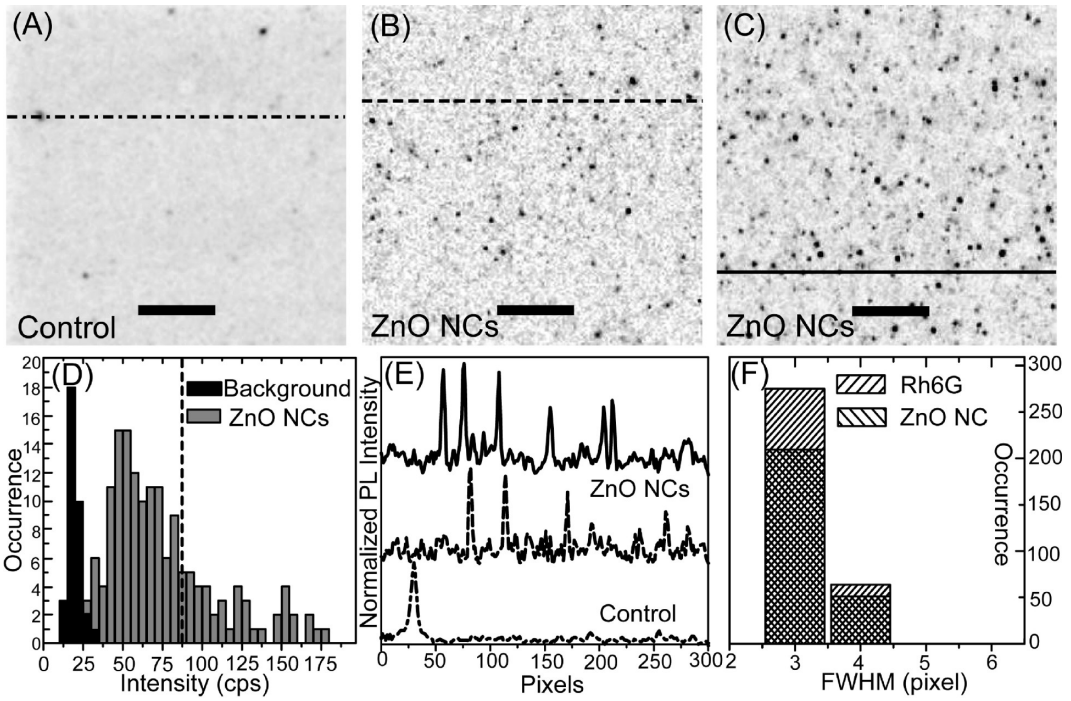

Figure 2. PL microscopy images of (A) control, (B) ~400 pM ZnO NCs, and (C) ~2 nM ZnO NCs. (Scale bar is 4 μm.) (D) PL intensity distributions of individual ZnO NCs (gray) and that of the background. (E) Intensity line profiles along the images in A (dashed), B (dashed-dotted), and C (solid). (F) fwhm of individual spots originating from ZnO NCs and single molecules of Rh6G.

imaging ZnO NCs. As a consequence, however, the individual luminescent spots were found to photobleach irreversibly within tens of seconds. PL intensity distribution analyses on 160 individual spots (and of the background) are shown in Figure 2D. Although most of the luminescent spots due to ZnO NCs have intensities typically 2−4 times that of the background, we do observe several spots that have relatively much higher intensities (beyond the vertical dashed line in Figure 2D). These bright spots are therefore attributed to clusters of NCs present within the same localized spot (i.e., in close proximity). The intensity line profiles of the control and for high and low concentration of ZnO samples are shown in Figure 2E. These indicate that the full-width at half maxima (fwhm) of almost all individual spatially separated spots in both Figure 2B and 2C are essentially ~3 pixels, which is the optical resolution of our PL microscopy setup. Spatial fwhm analyses of ~250 emission spots for the ZnO NCs and single Rh6G molecules (Figure 2F) demonstrate that the vast majority of the localized spots obtained in Figure 2B−C are diffraction-limited, suggesting that large aggregates of NCs are not formed under these experimental conditions. However, it should be kept in mind that spatial clustering of more NCs within a few tens of nanometers cannot be ruled out completely and is likely to be the case for the relatively bright diffraction limited spots (see Supporting Information, Figure S4 for PL image of ZnO aggregates).

Additional evidence of imaging individual NCs is obtained from temporal fluctuations of PL intensities of these luminescent spots upon continuous irradiation. Immobilized fluorescent molecules or quantum dots are expected to show emission intermittency with time (blinking) only at or near single-molecule/particle levels.[28,36,37] Figure 3 shows the blinking behaviors of six spatially isolated diffraction-limited spots typical of the ZnO NC sample. The PL emission from individual spots shows discrete

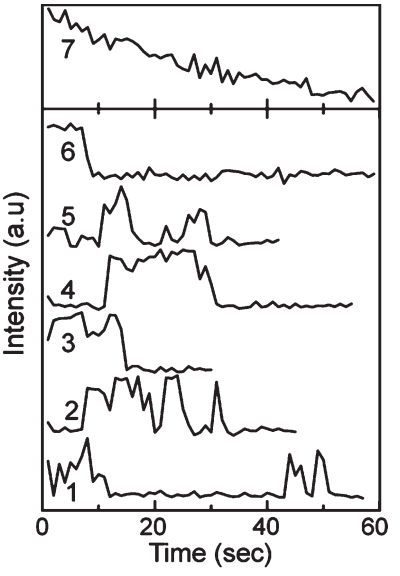

Figure 3. Temporal evolution of PL intensities (1 s bin) of six diffraction-limited spots due to ZnO NCs (traces 1−6). Trace 7 shows the same for a bright impurity observed in the control experiments. Aggregates of ZnO presumably having tens of NCs within the same spot also show similar behaviors as trace 7.

(quantized) jumps between two or more levels (traces 1−6), which are likely due to the formation of multiple charged states within the NCs.[36−38] It should be noted that the sequence of images was obtained at 1 s exposure time, and clear two-state blinking behaviors cannot be expected even at single-NC levels because the time scales of PL intermittency and data acquisition are comparable. However, the emission spots originating due to

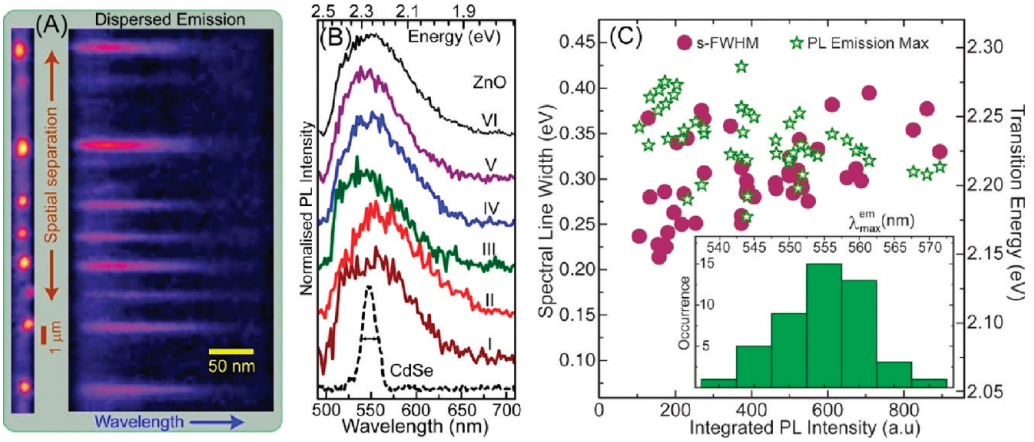

Figure 4. (A) Spectrally resolved PL imaging of ZnO NCs. The PL image through the slits is shown on the left, whereas the dispersed emission of the corresponding spots is shown on the right. (B) Solid lines show typical PL emission profiles of individual NCs (I−V), and the dotted line (VI) is the average of these five emission spectra. For comparison, the PL emission spectrum of a single CdSe quantum-dot (dashed line) having λ^{em}_{max} = 545 nm and s-fwhm (arrow) of 16 nm is shown. (C) Spectral line widths (circles) and corresponding transition energies (stars) are plotted as a function integrated PL intensities of individual spectra. The distribution of λ^{em}_{max} positions for 48 individual spectra is shown in the inset.

impurities (as well as for higher aggregates) typically show gradually diminishing PL intensities with irradiation times (see trace 7 of Figure 3). Therefore, the observed blinking behaviors as well as discrete (single- or multi-step) irreversible transition to an "off" state strongly suggest that each diffraction-limited spot contains a few NCs at the most, and it is unlikely that we probe the luminescence originating from larger clusters or higher aggregates of NCs.

Spectrally resolved PL imaging of individual ZnO NCs obtained using a combination of slit and transmission grating and their spectral analyses are shown in Figure 4. The zeroth order diffraction (i.e., image) of luminescent spots and their corresponding dispersed emission spectra (first-order image) obtained using the same CCD detector is shown in Figure 4A. The slit was chosen such that 5−10 luminescent spots spatially well-separated along the vertical direction could be imaged and spectroscopically resolved simultaneously. The dispersed emission shows up as horizontal streaks in the image, where the abscissa represents the wavelength scale. The emission spectra for every spatially separated diffraction-limited spot can be obtained by integrating along the vertical direction of each image. Even though wavelength resolution is slightly compromised, using a high transmission efficiency grating in conjunction with minimal optics in the detection path serves as an extremely useful method to obtain emission profiles efficiently. Note that the spectral resolution of our setup (∼5 nm) is determined by the spatial resolution of PL imaging rather than the resolution (70 lines/mm) of the grating (see Supporting Information).

Figure 4B shows the normalized PL spectral profiles of five different ZnO NCs (solid lines, I−V) and the average of the five individual emission spectra (dotted lines, VI) along with that of a single CdSe quantum-dot having excitonic emission at ∼550 nm. As compared to the PL emission of ZnO colloidal solution (Figure 1A, solid line), there is a slight red shift (∼10 nm; ∼40 meV) in the PL emission maxima (λ^{em}_{max}) position of the averaged spectra (VI). The lowering of peak energy positions is not surprising because only a part of the defect band is being excited, and a 500 nm long-pass filter is used to cut off the scattered light at high energies. However, each individual spectra differ from one another - some of the emission profiles (spectra III, V) show clear λ^{em}_{max} positions, whereas for many others (spectra I, II, IV) it was difficult to unambiguously locate the λ^{em}_{max} positions clearly, even after smoothing the raw data. Even though it often appears that there are two flanking peaks (or at least a shoulder) near the blue or red edge (spectra I−IV) of spectra, it was difficult to resolve these transitions with a high degree of confidence because of low energetic resolution and weak signal-to-background. Nonetheless, it is evident from Figure 4A,B that irrespective of the brightness of each spot observed through the slits, the defect λ^{em}_{max} positions of all ZnO NCs are clustered within a certain energetic window.

The analyses of 48 spectral profiles having relatively clear λ^{em}_{max} positions are shown in Figure 4C, which demonstrates that transition energies and spectral line widths (s-fwhm) are not correlated with the integrated PL emission intensities obtained from each diffraction limited spot. It should be noted that in Figure 4C each value of transition energy (open stars) is associated with a corresponding s-fwhm (filled circles) located vertically of each other, which are also found to be independent of each other. The distribution of λ^{em}_{max} positions shown as an inset of Figure 4C reiterates that transition energies of individual NCs are located within 540 and 570 nm (∼2.17 to 2.29 eV), having an energetic spread of ∼120 meV. The fluctuation of transition energies from one particle to another is likely to be a consequence of NC size distribution because it is known that carriers present in the defect states also show a quantum-confinement effect, resulting in shifting of their energies alongside VB/CB upon changing NC diameters.[18,35] However, the variation in the population of surface or native defects (i.e., defect density) upon changing NC dimensions may also contribute toward the shift in λ^{em}_{max} positions from one particle to another.[19,39] It is interesting to note that the size distributions obtained from TEM measurements (Figure 1B) reveal that NC diameters can vary from 4.4 to 5.8 nm, corresponding to which the defect emission maxima (in the ensemble) red shift by ∼100 meV (Supporting Information Figure S3). This is in reasonably good agreement with the observed fluctuation of transition energies for individual particles. It should be pointed out, however, that additional shift in transition energies of ∼30 meV, i.e., slight alteration of the defect energy levels, can

also arise from inhomogeneities in the local nanoenvironment in which individual NCs reside.[26,38]

Interestingly, irrespective of their transition energies, almost all single-particle emission profiles are found to span over the range of 510 and 630 nm, indicating that their spectral linewidths are not narrow. Typically, the s-fwhm for excitonic transitions of individual luminescent NCs such as CdSe quantum-dots (Figure 4B, dashed line) obtained in our experimental setup is ∼15 nm (∼70 meV) even at room temperature. In comparison, the s-fwhm for the defect emission of ZnO NCs was found to vary between 200 and 400 meV (Figure 4C). Even though there was no clear correlation between λ_{max}^{em} positions and the s-fwhm for individual NCs, bright spots typically have emission line widths slightly larger (50−100 meV) as compared with the mean value (300 meV). Therefore, the possibility of the presence of several ZnO NCs within these intense diffraction-limited spots cannot be ruled out. However, the PL spectra obtained from the least intense spots were always found to have s-fwhm of ∼200 meV or more, which points out that the defect emission line widths of individual ZnO NCs are broader than those of excitonic transitions observed for quantum dots.

The inherently broad line widths of this defect emission in ZnO NCs therefore indicate that the luminescence originating from the deep defect levels, V_0^+ (Figure 1C, solid vertical lines), have a continuous distribution of emissive states. These measurements also suggest that inhomogeneous broadening, i.e., energetic shifts due to quantum confinement of carriers, variation of defect density along with interfacial effects can contribute ∼130 meV to the overall spectral line widths of this visible defect band, at least for the samples prepared using aforesaid colloidal routes. Therefore, the entire defect emission band obtained in bulk solution, having line widths of ∼500 meV or more (Figure 1A), is also likely to be innately quite broad (∼350−450 meV), similar to those observed for high optical quality single-crystalline ZnO nanostructures with various morphologies.[8,9,40,41]

In summary, PL imaging and spectroscopy of colloidal ZnO NCs was performed near single-particle levels by selectively exciting the defect states. Spectrally resolved PL microscopy shows that the defect emission maxima of individual ZnO NCs occur near 550 nm, but the transition energies can vary up to ∼130 meV for different particles. More importantly, the spectral line width for the green-yellow defect emission is intrinsically broad, unlike those of excitonic transitions reported for individual semiconductor quantum dots. We observe that the contribution from inhomogeneous broadening to the spectra line widths is not pronounced, suggesting that the entire defect-related visible emission envelope for individual NCs is also likely to be innately broad (>350 meV). This work therefore further establishes the long-standing idea that multiple low-lying and closely spaced defect states form a quasi-band present in every ZnO NC, resulting in a continuous distribution of emissive states.

MATERIALS AND METHODS

ZnO NC Preparation and Characterization. A methanolic solution (75 mL) of KOH (0.48 g) was refluxed at 60 °C for 45 min in a temperature controlled reaction vessel. In another reaction mixture, 0.875 g $Zn(OAc)_2 \cdot 2H_2O$ was dissolved in 25 mL of methanol by sonication at room temperature. The zinc acetate solution was then injected dropwise into the refluxing KOH solution maintained at 60 °C by vigorous stirring, which resulted in the formation of ZnO NCs. To obtain different size of ZnO NCs, aliquots of the colloidal solution were taken out of reaction mixture at different time points and cooled to −10 °C in the presence of 1 mM of *tert*-butyl phosphonic acid (TBPA), which was used as a capping agent. This simple physicochemical route is found to be effective for preparing stable size-selected ZnO NCs having narrow size distributions. The synthesized NCs were characterized using UV−vis absorption, X-ray, and transmission electrical microscopy (TEM). Freshly prepared samples were used for all measurements.

Spectrally Resolved PL Microscopy. A home-built epi-fluorescence microscopy setup was used to perform spectrally resolved PL imaging of ZnO NCs. One drop of freshly prepared colloidal ZnO NCs (∼5 nm diameter) in methanolic solution was spin-cast at 2000 rpm on top of a cleaned fused-silica coverslip. A 488 nm Argon ion laser (Mellos Griot) was used to excite the sample placed on an inverted microscope (Nikon Eclipse 2000U). The expanded and collimated laser beam was focused on the back-focal plane of an oil immersion objective (60× 1.49NA Nikon) to illuminate ∼30 × 30 μm^2 area of the sample. The laser power before the entrance to the microscope was typically 30 mW. The emerging light was passed through a 488 nm dichroic mirror and notch filter (Semrock) and subsequently imaged using a cooled CCD camera (DVC) at 1 s of exposure time. PL emission profiles were obtained using a combination of a slit and a transmission grating (70 grooves/mm, Optometrics) placed before the CCD such that both the zeroth order (i.e., image) and first-order diffraction (i.e., spectra) could be obtained simultaneously. All emission profiles were obtained at 10 or 20 s of exposure time and analyzed after background flattening because of slight modulations in the excitation field. The spatial resolution of PL images; that is, fwhm of individual spots was ∼190 nm (3 pixels), whereas the spectral resolution was determined to be ∼5 nm. (See the Supporting Information.) The spectrally resolved images were corrected for the CCD detector response, and wavelength (pixel) positions were calibrated using three laser lines (488, 532, and 633 nm). The images were analyzed using ImageJ (NIH) and Origin. All measurements were performed at 295 K.

ASSOCIATED CONTENT

Supporting Information. Electron diffraction and X-ray diffraction patterns of ZnO NCs, bulk PL emission in solution, PL image of ZnO NCs aggregates, along with details of spectrally resolved PL microscopy setup and data analyses procedures are provided. This material is available free of charge via the Internet at http://pubs.acs.org.

AUTHOR INFORMATION

Corresponding Author

*Phone: +912225767154. Fax: +912225767152. E-mail: arindam@chem.iitb.ac.in, arunasish@chem.iitb.ac.in.

ACKNOWLEDGMENT

This work was partially supported by a grant from Council of Scientific and Industrial Research (CSIR), India (scheme no. 80(0070)/08/EMR-II) and IRCC, IIT-Bombay. S.D. and A.L.

thank CSIR and IIT-Bombay for their Ph.D. scholarships. The Department of Chemistry, SAIF, and Center for Research in Nanotechnology & Science (CRNTS) is acknowledged for usage of central facility instruments. We thank Drs. S. Dhar, G. Naresh-Patwari, and B. P. Singh for valuable discussions and critical review of the manuscript and S. Sapra for providing us with CdSe Quantum-Dot samples.

REFERENCES

(1) Huang, M. H.; Mao, S.; Feick, H.; Yan, H.; Wu, Y.; Kind, H.; Weber, E.; Russo, R.; Yang, P. Room-Temperature Ultraviolet Nanowire Nanolasers. *Science* **2001**, *292*, 1897–1899.

(2) Bera, D.; Qian, L.; Sabui, S.; Santra, S.; Holloway, P. H. Photoluminescence of ZnO Quantum Dots Produced by a Sol-Gel Process. *Opt. Mater.* **2008**, *30*, 1233–1239.

(3) Djurišić, A. B.; Leung, Y. H. Optical Properties of ZnO Nanostructures. *Small* **2006**, *2*, 944–961.

(4) Ruhle, S.; van Vugt, L. K.; Li, H. Y.; Keizer, N. A.; Kuipers, L.; Vanmaekelbergh, D. Nature of Sub-Band Gap Luminescent Eigenmodes in a ZnO Nanowire. *Nano Lett.* **2007**, *8*, 119–123.

(5) Tang, X.; Choo, E. S. G.; Li, L.; Ding, J.; Xue, J. Synthesis of ZnO Nanoparticles with Tunable Emission Colors and Their Cell Labeling Applications. *Chem. Mater.* **2010**, *22*, 3383–3388.

(6) Wu, Y. L.; Lim, C. S.; Fu, S.; Tok, A. I. Y.; Lau, H. M.; Boey, F. Y. C.; Zeng, X. T. Surface Modifications of ZnO Quantum Dots for Bio-Imaging. *Nanotechnology* **2007**, *18*, 215604/1–215604/9.

(7) Xiong, H.; Xu, Y.; Ren, Q.; Xia, Y. Stable Aqueous ZnO@ Polymer Core-Shell Nanoparticles with Tunable Photoluminescence and Their Application in Cell Imaging. *J. Am. Chem. Soc.* **2008**, *130*, 7522–7523.

(8) Ghosh, M.; Raychaudhuri, A. K. Shape Transition in ZnO Nanostructures and Its Effect on Blue-Green Photoluminescence. *Nanotechnology* **2008**, *19*, 445704/1–445704/7.

(9) Djurišić, A. B.; Leung, Y. H.; Tam, K. H.; Ding, L.; Ge, W. K.; Chen, H. Y.; Gwo, S. Green, Yellow, and Orange Defect Emission from ZnO Nanostructures: Influence of Excitation Wavelength. *Appl. Phys. Lett.* **2006**, *88*, 103107/1–103107/3.

(10) Ahn, C. H.; Kim, Y. Y.; Kim, D. C.; Mohanta, S. K.; Cho, H. K. A Comparative Analysis of Deep Level Emission in ZnO Layers Deposited by Various Methods. *J. Appl. Phys.* **2009**, *105*, 013502/1–013502/5.

(11) Norberg, N. S.; Gamelin, D. R. Influence of Surface Modification on the Luminescence of Colloidal ZnO Nanocrystals. *J. Phys. Chem. B* **2005**, *109*, 20810–20816.

(12) Bohle, D. S.; Spina, C. J. Cationic and Anionic Surface Binding Sites on Nanocrystalline Zinc Oxide: Surface Influence on Photoluminescence and Photocatalysis. *J. Am. Chem. Soc.* **2009**, *131*, 4397–4404.

(13) Lannoo, M.; Bourgoin, J. *Point Defects in Semiconductors: Experimental Aspects*. Springer: Berlin, 1983; Vol. 2.

(14) Lima, R. C.; Macario, L. R.; Espinosa, J. W. M.; Longo, V. M.; Erlo, R.; Marana, N. L.; Sambrano, J. R.; dos Santos, M. L.; Moura, A. P.; Pizani, P. S.; Andres, J.; Longo, E.; Varela, J. A. Toward an Understanding of Intermediate- and Short-Range Defects in ZnO Single Crystals. A Combined Experimental and Theoretical Study. *J. Phys. Chem. A* **2008**, *112*, 8970–8978.

(15) Borseth, T. M.; Svenssonm, B. G.; Kuznetsov, A. Y.; Klason, P.; Zhao, Q. Z.; Willander, M. Identification of Oxygen and Zinc Vacancy Optical Signals in ZnO. *Appl. Phys. Lett.* **2006**, *89*, 262112/1–262112/3.

(16) van Dijken, A.; Meulenkamp, E. A.; Vanmaekelbergh, D.; Meijerink, A. Identification of the Transition Responsible for the Visible Emission in ZnO Using Quantum Size Effects. *J. Lumin.* **2000**, *90*, 123–128.

(17) Rakshit, S.; Vasudevan, S. Trap-State Dynamics in Visible-Light-Emitting ZnO:MgO Nanocrystals. *J. Phys. Chem. C* **2008**, *112*, 4531–4537.

(18) Chakrabarti, S.; Ganguli, D.; Chaudhuri, S. Excitonic and Defect Related Transitions in ZnO−SiO_2 Nanocomposites Synthesized by Sol-Gel Technique. *Phys. Status Solidi A* **2004**, *201*, 2134–2142.

(19) Zhang, L.; Yin, L.; Wang, C.; Iun, N.; Qi, Y.; Xiang, D. Origin of Visible Photoluminescence of ZnO Quantum Dots: Defect-Dependent and Size-Dependent. *J. Phys. Chem. C* **2010**, *114*, 9651–9658.

(20) van Dijken, A.; Meulenkamp, E. A.; Vanmaekelbergh, D.; Meijerink, A. The Kinetics of the Radiative and Nonradiative Processes in Nanocrystalline ZnO Particles upon Photoexcitation. *J. Phys. Chem. B* **2000**, *104*, 4355–4360.

(21) Bohle, D. S.; Spina, C. J. The Relationship of Oxygen Binding and Peroxide Sites and the Fluorescent Properties of Zinc Oxide Semiconductor Nanocrystals. *J. Am. Chem. Soc.* **2007**, *129*, 12380–12381.

(22) Irimpan, L.; Nampoori, V. P. N.; Radhakrishnan, P.; Deepthy, A.; Krishnan, B. Size Dependent Fluorescence Spectroscopy of Nanocolloids of ZnO. *J. Appl. Phys.* **2007**, *102*, 063524/1–063524/6.

(23) Moerner, W. E. A Dozen Years of Single-Molecule Spectroscopy in Physics, Chemistry, and Biophysics. *J. Phys. Chem. B* **2002**, *106*, 910–927.

(24) Michalet, X.; Kapanidis, A. N.; Laurence, T.; Pinaud, F.; Doose, S.; Pfughoefft, M.; Weiss, S. The Power and Prospects of Fluorescence Microscopies and Spectroscopies. *Annu. Rev. Biophys. Biomol. Struct.* **2003**, *32*, 161–182.

(25) Kulzer, F.; Orrit, M. Single-Molecule Optics. *Annu. Rev. Phys. Chem.* **2004**, *55*, 585–611.

(26) Empedocles, S.; Bawendi, M. Spectroscopy of single CdSe Nanocrystallites. *Acc. Chem. Res.* **1999**, *32*, 389–396.

(27) Nirmal, M.; Brus, L. Luminescence Photophysics in Semiconductor Nanocrystals. *Acc. Chem. Res.* **1999**, *32*, 407–414.

(28) Nirmal, M.; Dabbousi, B. O.; Bawendi, M. G.; Macklin, J. J.; Trautman, J. K.; Harris, T. D.; Brus, L. E. Fluorescence Intermittency in Single Cadmium Selenide Nanocrystals. *Nature* **1996**, *383*, 802–804.

(29) Empedocles, S. A.; Bawendi, M. G. Quantum-Confined Stark Effect in Single CdSe Nanocrystallite Quantum Dots. *Science* **1997**, *278*, 2114–2117.

(30) Ong, H. C.; Du, G. T. The Evolution of Defect Emissions in Oxygen-Deficient and -Surplus ZnO Thin Films: The Implication of Different Growth Modes. *J. Cryst. Growth* **2004**, *265*, 471–475.

(31) Wang, X.; Zhao, F.; Xie, P.; Liang, S.; Deng, S.; Xu, N. Surface Luminescence in ZnO Nanoparticles. *Opt. Commun.* **2007**, *276*, 186–190.

(32) Wang, X.; Xie, P.; Zhao, F.; Wang, H.; Wang, Y. Spectra of ZnO Nanoparticles under Low Photon Energy Excitation. *Particuology* **2009**, *7*, 496–500.

(33) Viswanatha, R.; Sapra, S.; Satapati, B.; Satyam, P. V.; Dev, B. N.; Sarma, D. D. Understanding the Quantum Size Effects in ZnO Nanocrystals. *J. Mater. Chem.* **2004**, *14*, 661–668.

(34) Viswanatha, R.; Sarma, D. D. Study of the Growth of Capped ZnO Nanocrystals: A Route to Rational Synthesis. *Chem.—Eur. J.* **2006**, *12*, 180–186.

(35) Wood, A.; Giersig, M.; Hilgendorff, M.; Vilas-Campos, A.; Liz-Marzan, L. M.; Mulvaney, P. Size Effects in ZnO: The Cluster to Quantum Dot Transition. *Aust. J. Chem.* **2003**, *56*, 1051–1058.

(36) Wang, S.; Querner, C.; Fischbein, M. D.; Willis, L.; Novikov, D. S.; Crouch, C. H.; Drndic, M. Blinking Statistics Correlated with Nanoparticle Number. *Nano Lett.* **2008**, *8*, 4020–4026.

(37) Crouch, C. H.; Sauter, O.; Wu, X.; Purcell, R.; Querner, C.; Drendic, M.; Oelton, M. Facts and Artifacts of Single-Molecule Blinking Dynamics in Semiconductor Nanocrystals. *Nano Lett.* **2010**, *10*, 1692–1698.

(38) Dias, E. A.; Grimes, A. F.; English, D. S.; Khambhampati, P. Single Dot Spectroscopy of Two-Color Quantum Dot/Quantum Shell Nanostructures. *J. Phys. Chem. C* **2008**, *112*, 14229–14232.

(39) Zhao, Q. X.; Klason, P.; Willander, M.; Zhong, H. M.; Lu, W.; Yang, J. H. Deep-Level Emissions Influenced By O and Zn Implantations in ZnO. *Appl. Phys. Lett.* **2005**, *87*, 211912/1–211912/3.

(40) Rosa, E. D. l.; Sepúlveda-Guzman, S.; Reeja-Jayan, B.; Torres, A.; Salas, P.; Elizondo, N.; Jose Yacaman, M. Controlling the Growth

and Luminescence Properties of Well-Faceted ZnO Nanorods. *J. Phys. Chem. C* **2007**, *111*, 8489–8495.

(41) Jiao, Y.; Zhu, H. J.; Zhou, M. J.; Wang, X. F.; Li, Q. Suppression of Green Emission in ZnO Nanorodss-A Discussion on Surface and Interior Structural Quality Manipulation. *J. Phys. Chem. C* **2010**, *114*, 208–211.

Supporting Information

Spectrally Resolved Photoluminescence Imaging of ZnO Nanocrystals at Single-Particle Levels

*Arunasish Layek, Suman De, Ruhi Thorat, and Arindam Chowdhury**

1. Structural Characterization

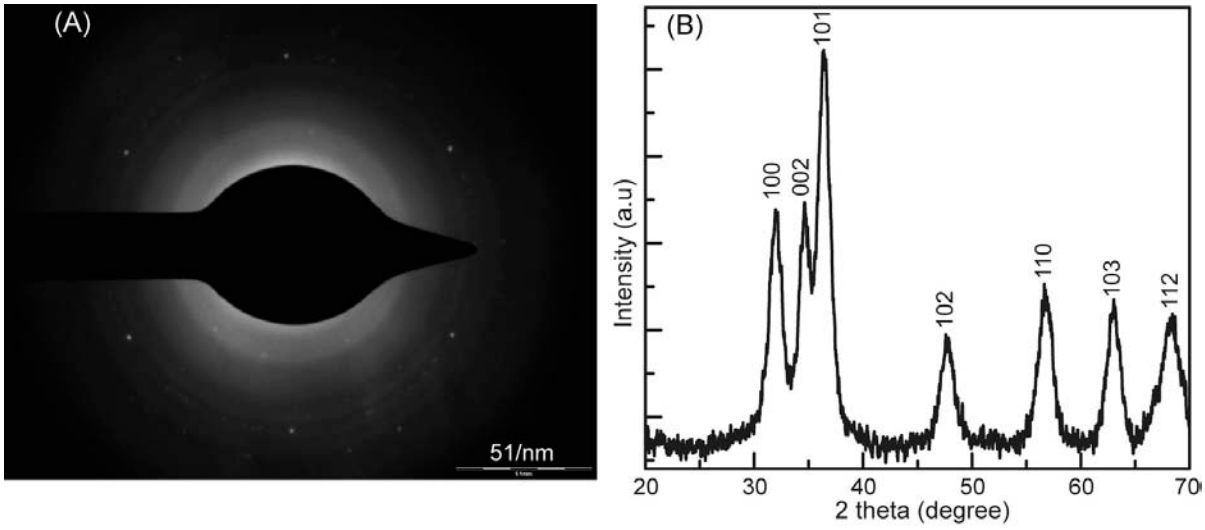

Figure S1. (A) Electron diffraction pattern indicates crystalline nature of ZnO NPs while (B) shows the X-ray diffraction pattern of ZnO NPs. The diffraction patterns clearly indicate the hexagonal wurtzite crystalline nature of the ZnO NCs.

The electron diffraction (ED) patterns (Figure S1. (A)) clearly shows the crystalline nature of the 5 nm ZnO NC samples. The powder X-ray diffraction (XRD) patterns of the ZnO NCs (Figure S1. (B)) could be easily indexed to the hexagonal wurtzite structure and in characteristic of ZnO.

Supporting Information

2. Spectrally Resolved PL Imaging Microscopy setup

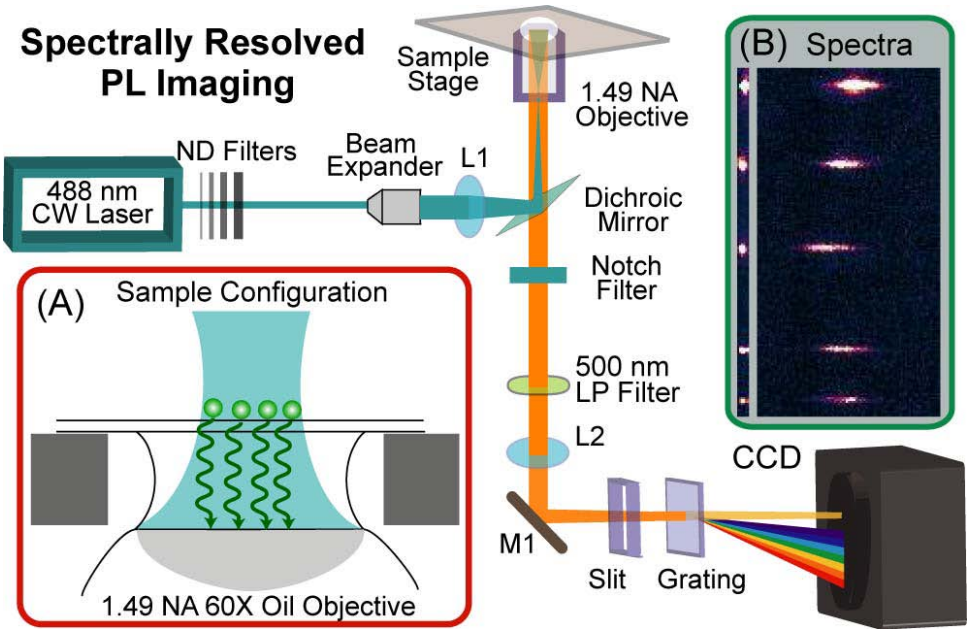

Figure S2. Schematic of experimental setup for single particle photoluminescence spectroscopy is shown. The sample configuration is magnified in insert (A) while (B) displays the dispersed emission profile obtained from individual dots.

Spectrally Resolved Photoluminescence Microscopy: Details of the home-built laser photoluminescence microscopy setup was used for spectrally resolved imaging of ZnO NCs is shown in Figure S2. The 488 nm line of an Ar+ laser (Mellos Griot) was used to selectively excite the deep level defects (V_o^+) of ZnO NCs in epi-fluorescence configuration (Figure S2, inset A) through an inverted microscope (Nikon Eclipse 2000U). The expanded and collimated laser beam was focused using a Plano-convex lens on the back-focal plane of the 60X, 1.49NA oil immersion objective lens (Nikon) to a spot of adjustable diameter. In general, 20-30 mW excitation power (at the back-entrance of the objective lens) was used to illuminate the sample area of 30x30 μm^2. The emerging photoluminescence was collected by the same objective and separated from the excitation beam by using a dichroic mirror (Semrock DI01-R488) and a 488nm notch filter (Semrock NF03-488E-25) and subsequently imaged using cooled CCD

camera (DVC-1412AM) at 1 sec exposure time. Temporal fluctuation of PL intensities, i.e. blinking behaviors was obtained by acquiring movies at 1s exposure. To obtain the PL spectra of individual spots, the emission was collected through a slit and a transmission grating (70 grooves/mm, Optometrics) mounted in front of the CCD. The distance between the transmission grating and the CCD was set such a way that 0^{th}-order diffraction (image) and 1^{st}-order diffraction (spectra) (Figure S2 inset B) would not spatially overlap and both the image and spectra would appear in the field of view of the CCD with high enough spatial resolution, i.e., the energetic spread of the emission between 500 and 700 nm occurs over ~150 pixels.

Data Analyses: All analysis of the images, time traces and spectra were done using freely available ImageJ (NIH) and Origin 8. All PL images were analyzed after background flattening using a rolling ball algorithm due to slight modulations in the excitation field unless otherwise mentioned. The spectrally resolved images were also analyzed by integrating 3 pixels along vertical directions to obtain the emission profiles, from which the average background was subtracted to obtain the spectra due to individual spots, and then corrected for the CCD detector response over the entire wavelength range (500-750 nm). The wavelength positions (with respect to CCD pixels) were calibrated using three laser lines: 488 nm, 532 nm and 633 nm, where the dispersion was found to be linear, and each pixel position along abcissa corresponded to 1.35 nm in wavelength position. Since the optical resolution of our microscope (i.e. the diffraction limit) is ~ 3 pixels, the minimum energetic resolution of our set up is no more than ~5 nm, which corresponds to ~20 meV in this wavelength range. While performing the pixel to wavelength (nm) conversion, have meticulously chosen the center of each luminescent spot in the 0^{th} order image from which the distance in pixel for the 1^{st} order images were measured, thereby minimizing the error due to variation of absolute location of individual particles within the slits. Each spectrum was fitted with a polynomial function in Origin and the peak positions and FWHM was obtained manually. However, it should be pointed out that due to weak signal to background and relatively wide emission envelope observed for each spatially separated diffraction-limited spot may also add slight error of ~10 meV in the estimation of both transition energies and spectral line-widths.

Supporting Information

3. Bulk PL of colloidal ZnO NCs under UV-excitation (λ_{ex}=325 nm)

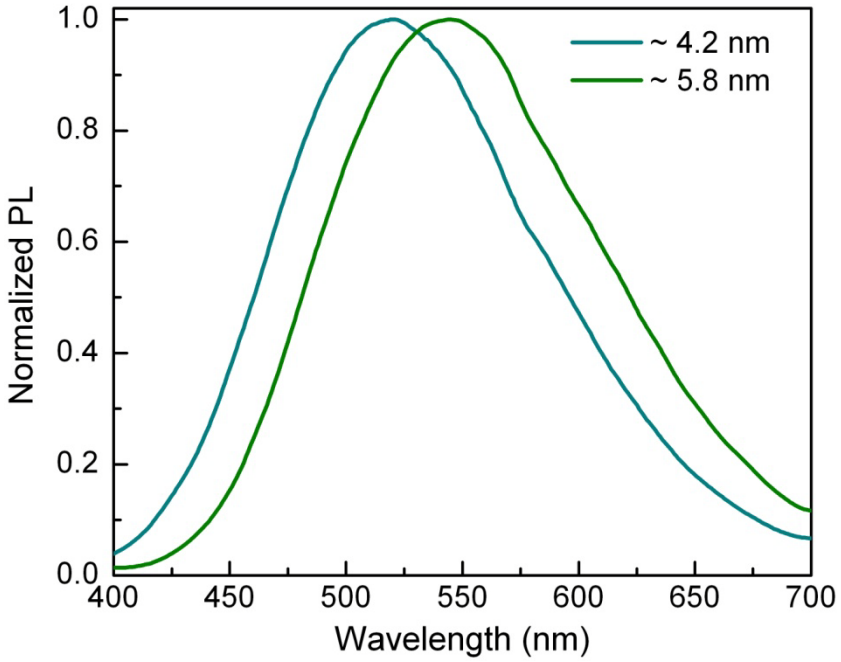

Figure S3. Shift in visible PL peak maxima positions due to change in size of ZnO NCs.

Shift of the defect PL due to NC dimensions. Figure S3 shows that with change in ZnO NCs size there is a concomitant shift of defect mediated visible luminescence band. Due to change in particle size from ~ 4.2 nm to ~5.8 nm there is shift in $\lambda_{\max}^{em}$ from 520 nm to 545 nm (~110 meV). For the ZnO sample having size distribution from 4.3 to 5.8 nm (Figure 1B), we observe that the single particle PL maxima positions vary over ~130 meV from one particle to the other (Figure 4C). This observed energetic shift of ~110 meV is consistent with our proposition that transition energy variation in individual ZnO NCs is due to particle size distribution in our sample.

Supporting Information

4. PL Microscopy of high conc. ZnO NCs under 488 nm Laser Excitation:

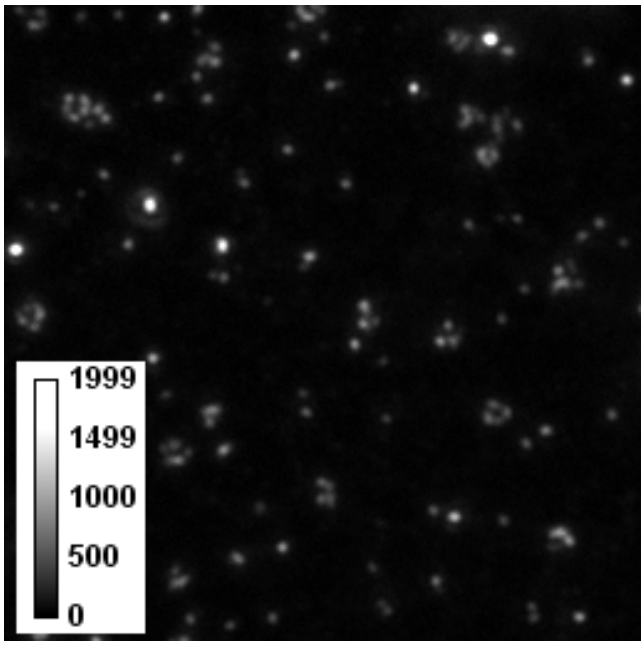

Figure S4. PL image of aggregated ZnO NCs under 488 nm laser excitation. The image dimension is ~16 μm.

PL microscopy of ZnO aggregates. When freshly prepared high conc. ZnO NCs (1-2 μM) is spin casted on top of glass coverslip, we obtain mostly aggregated spots. The aggregated ZnO NCs when excited with 488 nm with laser power 20 mW and images collected at 100 ms exposure, we observe that most of luminescent spots are very intense. Additionally, many of these intense spots are non-diffraction limited. The intensity of the luminescent centers varies from 1000-2000 counts, i.e. 10000-20000 cps. If we assume that there is approximately 1000 particles aggregated in each spots, the intensity corresponding to single NCs should be ~ 10-20 counts. We have observed similar intensities when we recorded the PL image for 2 nM ZnO NCs using 488 nm excitation for identical excitation powers at 1s exposure times.